Ten Interventional Oncology Pearls

Positive outcomes and useful technical tips for a successful oncology practice.

BY NICHOLAS FIDELMAN, MD; MATTHEW D. BUCKNOR, MD; PAUL HASTE, MD; MAUREEN P. KOHI, MD; RYAN M. KOHLBRENNER, MD; K. PALLAV KOLLI, MD; KRISTEN LEE, MD; EVAN D. LEHRMAN, MD; THOMAS M. LINK, MD, PHD; AND ANDREW G. TAYLOR, MD, PHD

1. MIRACLES HAPPEN

A 65-year-old woman with hepatitis C virus (HCV) infection underwent routine laboratory testing, which showed an elevated alpha-fetoprotein (AFP). Multiphase contrast-enhanced CT showed liver and left adrenal masses (Figure 1A and 1B). An adrenal mass biopsy revealed poorly differentiated hepatocellular carcinoma (HCC). Two transarterial chemoembolization (TACE) procedures were performed 1 month apart using doxorubicin, mitomycin C, cisplatin, ethiodized oil, and gelatin sponge slurry, which targeted both the liver and left adrenal masses. Follow-up cross-sectional imaging studies and AFP testing obtained over a 6-year period have shown no HCC recurrence (Figure 1C–E).

TACE is the recommended treatment for Barcelona Clinic Liver Cancer stage B HCC. Rarely, local therapies have been employed for treatment of oligometastatic HCC, especially to the adrenal glands.[1] Local and distant recurrences are typical. However, on rare occasion, remission of locally advanced and metastatic HCC after local therapy has been reported.[2]

2. REMEMBER THE EXTRAHEPATIC COLLATERALS

A 63-year-old man with a previously treated solitary right liver lobe HCC developed local recurrence and was referred for repeat TACE. Cone-beam CT obtained during contrast injection via the right hepatic artery demonstrated no enhancement of a posterior aspect of the right liver lobe known to contain the tumor, which suggested that the tumor had recruited extrahepatic

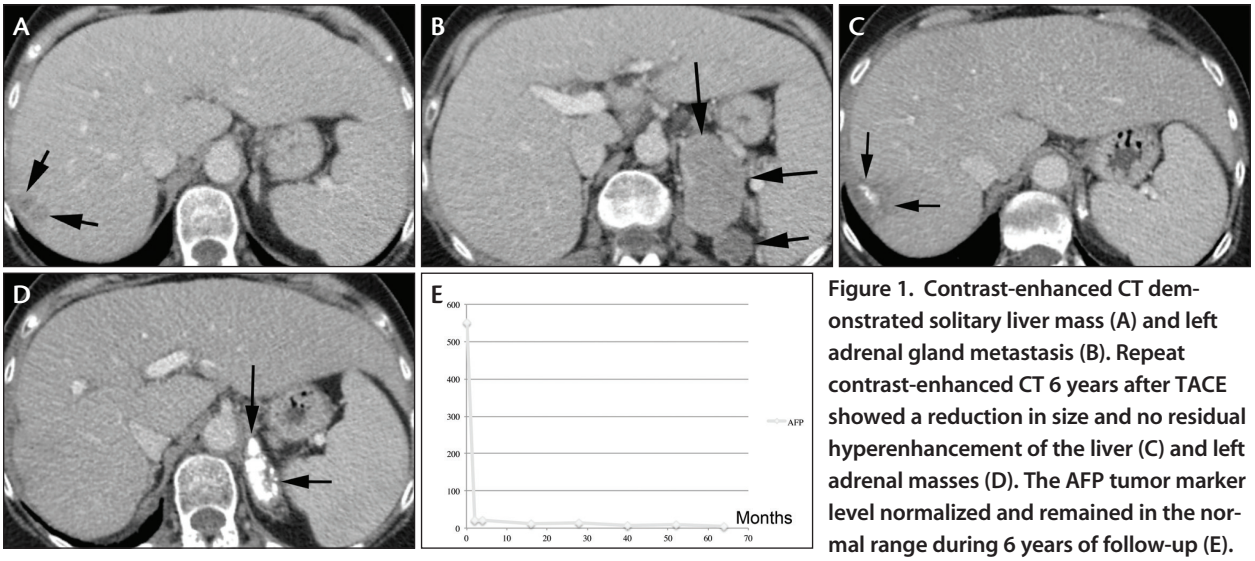

Figure 1. Contrast-enhanced CT demonstrated solitary liver mass (A) and left adrenal gland metastasis (B). Repeat contrast-enhanced CT 6 years after TACE showed a reduction in size and no residual hyperenhancement of the liver (C) and left adrenal masses (D). The AFP tumor marker level normalized and remained in the normal range during 6 years of follow-up (E).

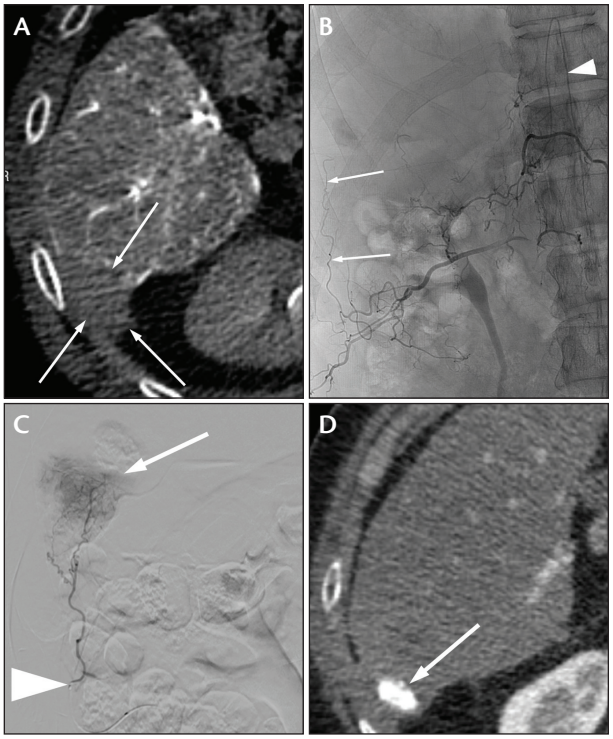

Figure 2. Cone-beam CT of the right hepatic artery demonstrated a paucity of artery supply (A, arrows) to an LI-RADS category 5 HCC in a patient who had received previous chemoembolization. Multiple intercostal and lumbar arteries were interrogated using angiography until the 12th intercostal artery that supplied the tumor was identified (B, arrows). Note the artery of Adamkiewicz arising from the proximal portion of the 12th intercostal artery (B, arrowhead). Advancing a microcatheter distally (C, arrowhead) into the branch supplying the tumor (arrow) allowed for safe administration of TACE. Follow-up CT showed retention of ethiodized oil in the treated tumor (D, arrow) corresponding to the area of nonperfusion identified on the original cone-beam CT Scan.

arteries (Figure 2A). Digital subtraction angiography (DSA) of the right 12th intercostal artery showed small branches of a right intercostal artery extending to the liver (Figure 2B) that supplied the hypervascular liver tumor (Figure 2C). Follow-up CT showed accumulation of ethiodized oil in the liver lesion supplied by a branch of the intercostal artery (Figure 2D).

Primary and metastatic liver tumors usually derive blood supply from the hepatic artery. However, several scenarios increase the likelihood of parasitized tumor supply, including large size, subcapsular location, previous intrahepatic artery embolization, previous surgery, and rupture.[3] Familiarity with common extraheptic artery sources is important for performing effective arterial liver therapies. Cone-beam CT can be used to exclude hepatic artery supply (Figure 2A). Depending on the location of the tumor within the liver, various arterial distributions can be interrogated. When the tumor is near the dome, the inferior phrenic artery should be evaluated. Posterior tumors may recruit intercostal or lumbar arteries (Figure 2B). Less common sources include the internal mammary, omental, renal, adrenal, and cystic arteries. After careful evaluation of the angiogram, chemoembolization may safely be performed into these extrahepatic tumor feeders. Injection of selective internal radiation therapy with yttrium-90 microspheres into extrahepatic tumor feeders has been reported but remains controversial.[4] Consideration can be given to bland embolization of extrahepatic feeders with large particles and coils to redistribute flow back into the liver before radioembolization.

3. OMENTAL ARTERIES MATTER

A 69-year-old woman with an 8-cm, exophytic, biopsy-proven HCC in segment 5 of the liver presented for repeat TACE after surveillance imaging detected residual viable tumor (Figure 3A). A common hepatic angiogram demonstrated vascular supply to the inferior aspect of the mass from an omental branch arising from the gastroduodenal artery (Figure 3B). After superselective catheterization of the omental branch, angiography again confirmed vascularity to the inferior aspect of the mass

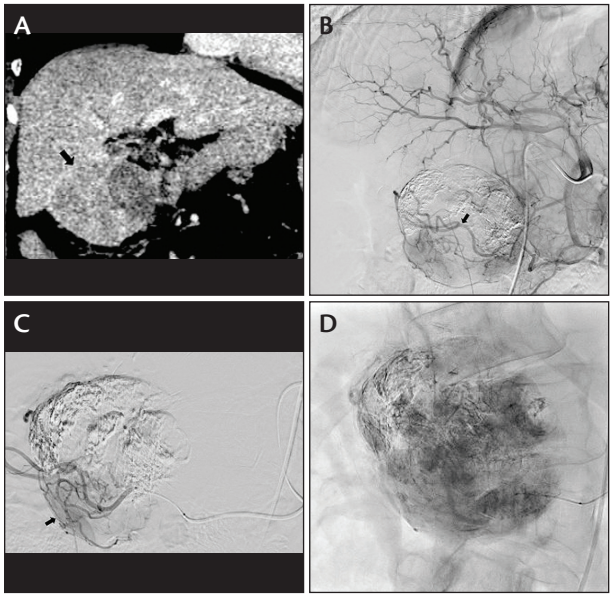

Figure 3. Contrast-enhanced CT coronal reformation after TACE for exophytic right liver lobe HCC (A). Gastroduodenal artery (B) and omental branch (C) angiograms confirmed omental artery supply to the viable portion of the tumor. A fluoroscopic spot image demonstrated accumulation of ethiodized oil within the embolized portion of the mass after TACE (D).

(Figure 3C). Chemoembolization was performed using a combination of 25 mg doxorubicin, 10 mg mitomycin C, ethiodized oil, and gelatin sponge slurry (Figure 3D).

The omental arteries are a common extrahepatic arterial supply to HCC[5] and tend to supply tumors that are exophytic or at the surface of the right hepatic lobe and the medial segment of the left lobe.[6] Performing TACE through omental artery branches is usually safe, with postembolization syndrome reported as the most common toxicity. Serious complications such as omental infarction and fat necrosis are relatively uncommon.[7]

It should be noted that it may be difficult to detect omental artery supply to HCC with CT because of the variability and tortuosity of the arterial course. Therefore, when there is a high index of suspicion for extrahepatic artery supply, gastroduodenal angiography should be considered to detect HCC artery supply from omental branches.[5]

4. SUPERIOR MESENTERIC ARTERY COLLATERALS SAVE THE DAY

A 53-year-old patient presented for chemoembolization of two segment 8 hepatic lesions classified as Liver Imaging Reporting and Data System (LI-RADS) category 5 (Figure 4). However, due to the near-occlusion of the proximal celiac axis, access to the hepatic arteries was obtained in a retrograde fashion via the superior mesenteric artery (SMA). Abdominal aortography was performed, which confirmed near occlusion of the celiac axis, with retrograde filling of the hepatic arteries via a robust pancreaticoduodenal arcade (PDA). To provide additional stability for catheterization through the tortuous arcade, a triaxial system was used. A 6-F, renal double-curve (Vista Brite Tip, Medtronic) sheath was placed at the ostium of the SMA with a 4-F Glidecath catheter (Terumo Interventional Systems) manipulated through the PDA branch of the SMA to the level of the common hepatic artery. The hepatic arteries were selectively catheterized using a microcatheter for chemoembolization.

The PDA and the dorsal pancreatic artery are the most common and important collateral pathways from the SMA for patients with occlusion or hemodynamically significant stenosis of the celiac axis due to atherosclerotic disease or median arcuate ligament.[8]

5. SPARE THE DIAPHRAGM

A 61-year-old man with hepatitis C cirrhosis and HCC, who previously underwent TACE, was diagnosed with a 4-cm recurrent mass in segment 8 noted on follow-up MRI (Figure 5A) and was referred for percutaneous microwave ablation. Using intermittent CT guidance, a microwave antenna (Emprint, Medtronic) was advanced into the lesion. Two 10-minute, 100-W ablations were performed in overlapping areas of segment 8 adjacent to the right hemidiaphragm (Figure 5B). There

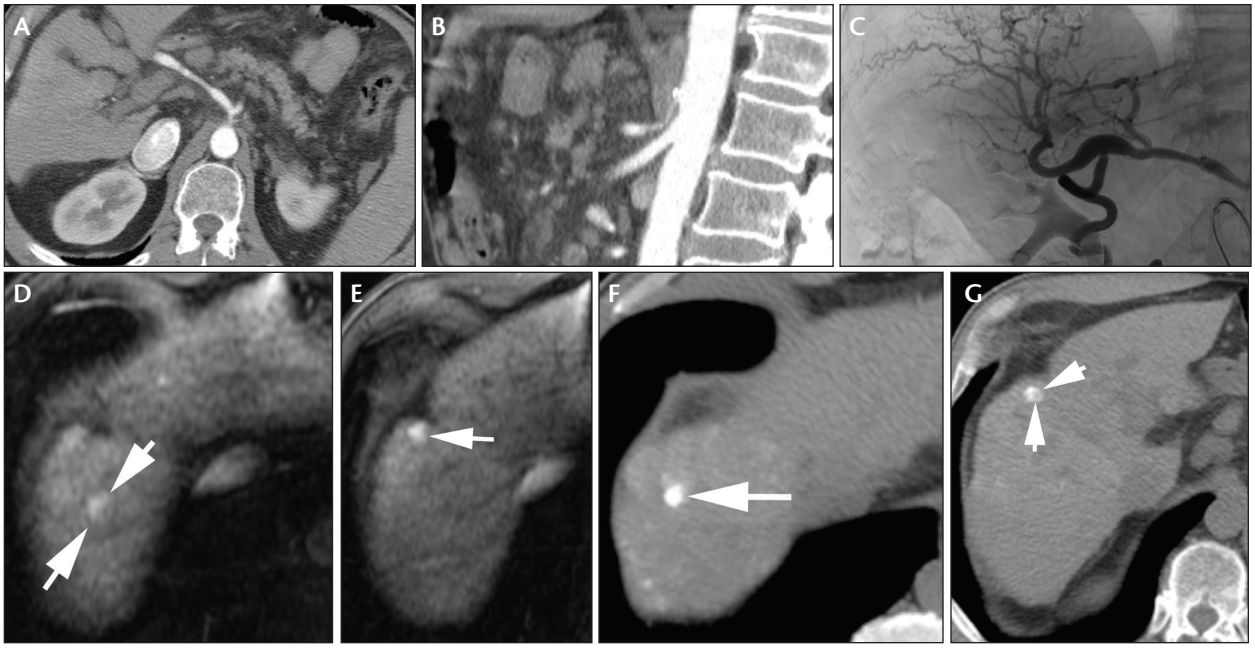

Figure 4. Axial (A) and sagittal (B) contrast-enhanced CT demonstrated near occlusion of the proximal celiac artery. The PDA branch of the SMA was selectively catheterized using a triaxial system, demonstrating a robust PDA, which allowed retrograde filling of the hepatic arteries (C). Axial MRI images before treatment demonstrated two LI-RAD category 5, segment 8 lesions (D, E). Axial noncontrast-enhanced posttreatment CT images demonstrated ethiodized oil uptake in the two treated lesions (F, G).

Figure 5. Axial, dynamic, contrast-enhanced, fat-saturated, T1-weighted MRI image demonstrated a hypervascular mass in the hepatic dome (A). Axial intraprocedural noncontrast-enhanced CT image demonstrated a radiodense microwave antenna probe in the expected region of the tumor's anterolateral aspect (B). The right hemidiaphragm was approximately 1 cm away. Axial postcontrast CT scan obtained 1 month after ablation demonstrated extension of the ablation cavity to the intact diaphragm (C).

were no immediate or delayed complications. Follow-up CT scan performed 1 month after ablation demonstrated an ablation cavity abutting the intact right hemidiaphragm and no evidence of residual disease (Figure 5C).

Ablating lesions in the hepatic dome may be challenging due to poor ultrasound visualization or the steep probe angulation required during CT-guided placement. However, if the lesion can be reached from a percutaneous approach, microwave ablation is considered both safe and effective for hepatic dome lesions near the diaphragm. One recent study showed no cases of diaphragmatic hernia identified on follow-up, and the likelihood of local recurrence was not significantly higher than in other areas of the liver.[9]

6. MAKING IMPOSSIBLE POSSIBLE: ANGLING THE CT GANTRY

A 66-year-old cirrhotic patient presented with HCC high in segment 2, just below the diaphragm (Figure 6A and 6B). The patient was placed under general anesthesia during a CT-guided ethanol ablation procedure, with apnea of the lesion (arrows, Figure 6C and 6D) well above the costal margin. Both the anterior ribs and the heart prevented a straightforward axial approach. The CT gantry was angled 22.5° caudally to improve the imaging and allow for visualization of the entire needle pass in a single axial slice (Figure 6E and 6F). This improved the ease and accuracy of the needle placement and subsequent injection of alcohol into the tumor (dark area at the needle tip, Figure 6E). Note the very different appearance of the ribs at the new angle.

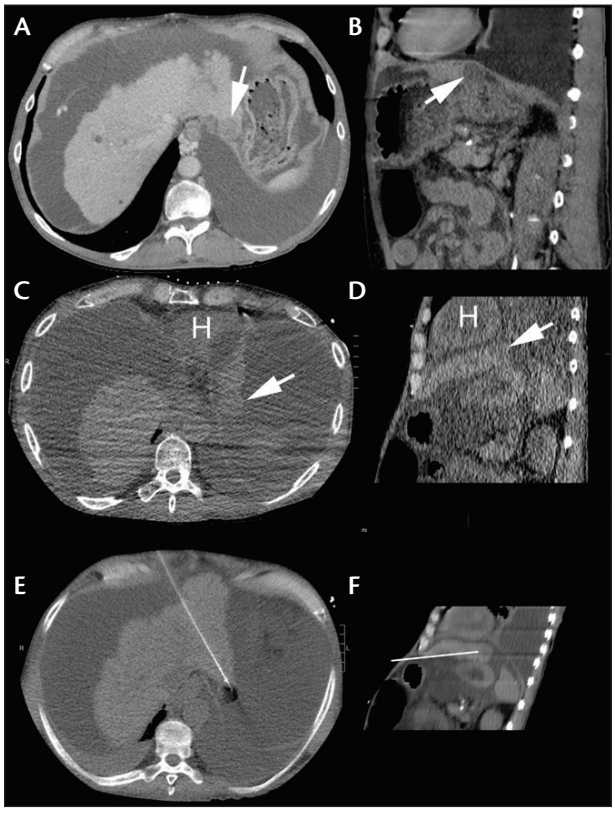

Figure 6. Axial (A) and sagittal reformat (B) contrast-enhanced CT obtained in inspiration. Axial (C) and sagittal reformat (D) noncontrast-enhanced CT obtained during apnea when patient was placed under general anesthesia. Axial (E) and sagittal reformat (F) CT obtained after angling the gantry 22.5° caudally.

7. CONTRAST-ENHANCED ULTRASOUND IMPROVES LIVER LESION VISUALIZATION

A 59-year-old man with HCV cirrhosis and HCC treated with multiple TACE and thermal ablations presented with a small, enhancing liver tumor and elevated AFP levels (Figure 7A). A previously attempted ethanol ablation had been unsuccessful because of difficulty with exact targeting of the tumor with CT. A contrast-enhanced ultrasound (SonoVue, Bracco Imaging) was used to visualize the tumor. Although the lesion was

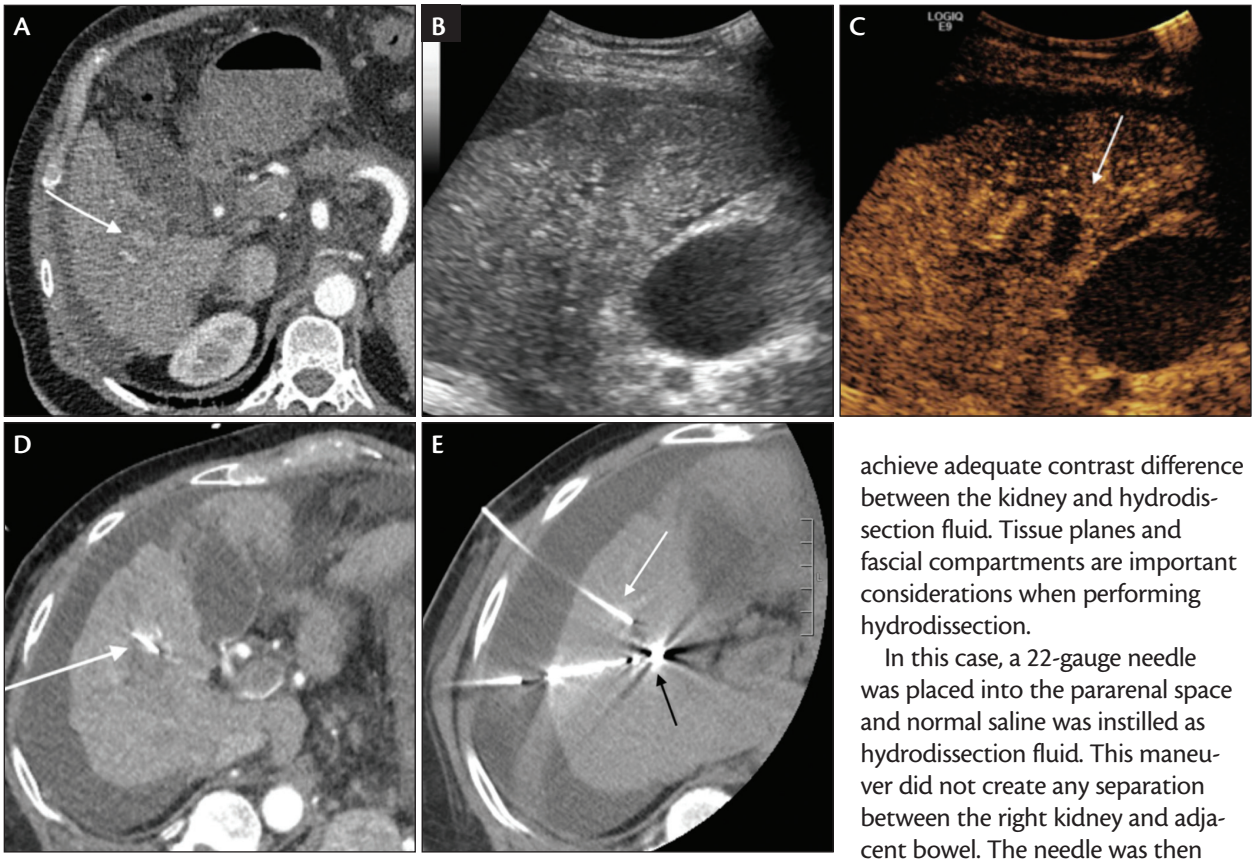

Figure 7. Arterial-phase CT demonstrated small enhancing tumor (A, white arrow) surrounded by parenchymal changes related to prior treatment. Grayscale ultrasound poorly demonstrated the tumor (B). Delay-phase contrast-enhanced ultrasound demonstrated clear washout (C, white arrow). CT during ablation with 22-gauge Chiba needle (D, white arrow) placed directly into the viable tumor using contrast-enhanced ultrasound guidance. CT during ablation showed microwave probe (E, black arrow) positioned using the 22-gauge Chiba needle (white arrow) as a landmark.

difficult to see on grayscale ultrasound (Figure 7B), the delayed phase (Figure 7C) of the contrast-enhanced ultrasound allowed for more accurate targeting. With ultrasound guidance, a 22-gauge Chiba needle (Cook Medical) was advanced into the lesion (Figure 7D). That needle tip was then used to guide placement of a microwave ablation probe (Figure 7E).

8. HYDRODISSECT TO AVOID COLON INJURY

A 30-year-old woman with a history of von Hippel-Lindau disease was referred for percutaneous cryoablation of an enlarging 2-cm endophytic right renal mass (Figure 8A). A nephron-sparing approach was strongly preferred in this young patient with a history of multiple other small bilateral renal tumors. A 3:100 solution of contrast medium in normal saline can be instilled to achieve adequate contrast difference between the kidney and hydrodissection fluid. Tissue planes and fascial compartments are important considerations when performing hydrodissection.

In this case, a 22-gauge needle was placed into the pararenal space and normal saline was instilled as hydrodissection fluid. This maneuver did not create any separation between the right kidney and adjacent bowel. The needle was then carefully repositioned into a very tight window between the kidney and adjacent bowel with the intention of instilling hydrodissection fluid into the retroperitoneum in either the anterior pararenal space or perirenal space (Figure 8B). Fluid instilled through a needle in this location pooled anteriorly in the peritoneum (Figure 8C). With final repositioning of the needle into a seemingly less advantageous position adjacent to the kidney, hydrodissection fluid accumulated in the perirenal space of the retroperitoneum (Figure 8D). Adequate separation between kidney and bowel was achieved to allow subsequent cryoablation without risk of thermal injury to bowel. This case illustrates the utility of hydrodissection in separating the kidney from adjacent structures during percutaneous renal mass cryoablation.

9. HIGH-INTENSITY FOCUSED ULTRASOUND PALLIATES BONE PAIN

A 42-year-old woman with history of metastatic colon cancer, including metastasis to the left intertrochanteric and subtrochanteric femur, had persistent pain at that site despite previous external beam radia-

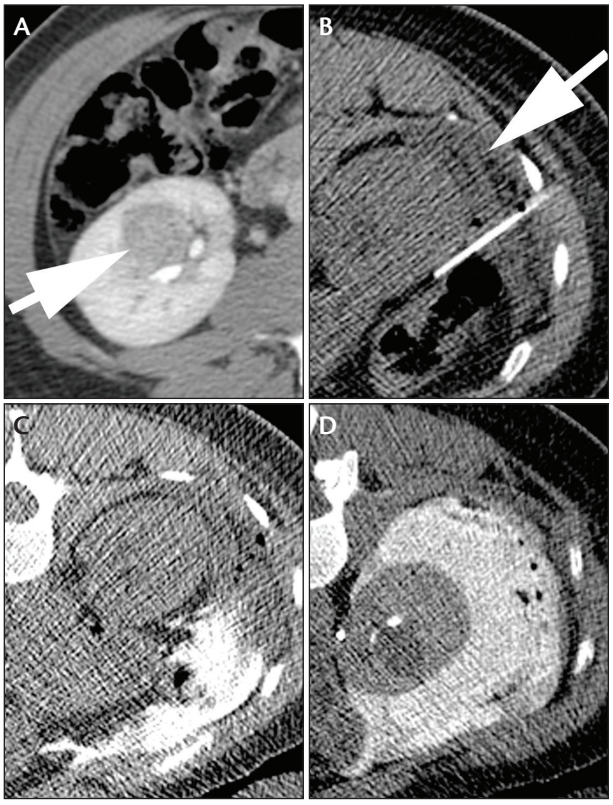

Figure 8. Contrast-enhanced CT image of the enlarging right renal mass (A, arrow) with < 1 cm distance between anterolateral tumor margin and the hepatic flexure of the colon. Initial instillation of normal saline hydrodissection fluid (B, arrow) into the pararenal space did not result in separation between the right kidney and bowel. Therefore, a 22-gauge needle was advanced into the fat between the right kidney and the hepatic flexure. Hydrodissection fluid (now using 3:100 dilution of Omnipaque 350 [GE Healthcare] contrast media in normal saline) instilled with the needle in this location pooled dependently in the peritoneum (C). The 22-gauge needle has been repositioned (D) into a seemingly less advantageous position with tip adjacent to the kidney rather than between the kidney and adjacent bowel. However, fluid instilled through the needle in this position accumulated in the perirenal space and created separation from adjacent bowel.

tion treatment. The patient received ongoing chemotherapy, and despite improvement in tumor marker that suggested response to therapy, she continued to have significant pain correlating with this site of osseous metastatic disease (6 on a 1–10 scale). Pain medication regimen included morphine 15 mg twice daily. The patient was referred for magnetic resonance (MR)–guided focused ultrasound, which was performed with 11 sonications. Temperature varied from approximately 70° to 90° C during the sonications with

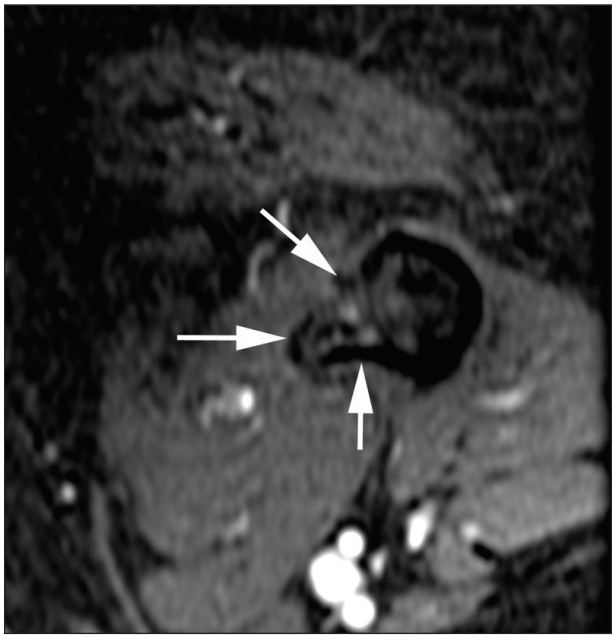

Figure 9. Axial spoiled gradient echo postcontrast MRI demonstrated black box appearance of hypoenhancement along the bone/soft tissue interface (arrows) following MR-guided focused ultrasound of a colon cancer metastasis to the proximal left femur.

up to 5,000 J in total energy per sonication. Each individual sonication was 20 seconds.

Postcontrast imaging immediately after ablation demonstrated the "black box" appearance of hypoenhancement along the bone/soft tissue interface, which correlates with ablation of periosteal nerves and a better chance of improvement in patient's pain (Figure 9).[10] Three days after MR-guided focused ultrasound, pain had resolved and the patient was able to discontinue the morphine regimen.

10. CURE OSTEOID OSTEOMA WITH ABLATION

A 12-year-old girl developed chronic pain in the left thigh and knee. After several weeks of symptoms, plain radiographs of the left femur were obtained, which demonstrated a focal area of cortical thickening with central lucency (Figure 10A), consistent in appearance with an osteoid osteoma. Treatment with nonsteroidal anti-inflammatory medication did not alleviate the pain completely. Narcotics were required for breakthrough pain. Therefore, the patient underwent radiofrequency ablation approximately 9 months after symptoms had developed.

The procedure was performed under general anesthesia, as the osteoid osteoma nidus is extremely painful for intervention and the ablation heats up the periosteum, which also causes severe pain. With the patient in a prone position, the entrance site for the procedure was

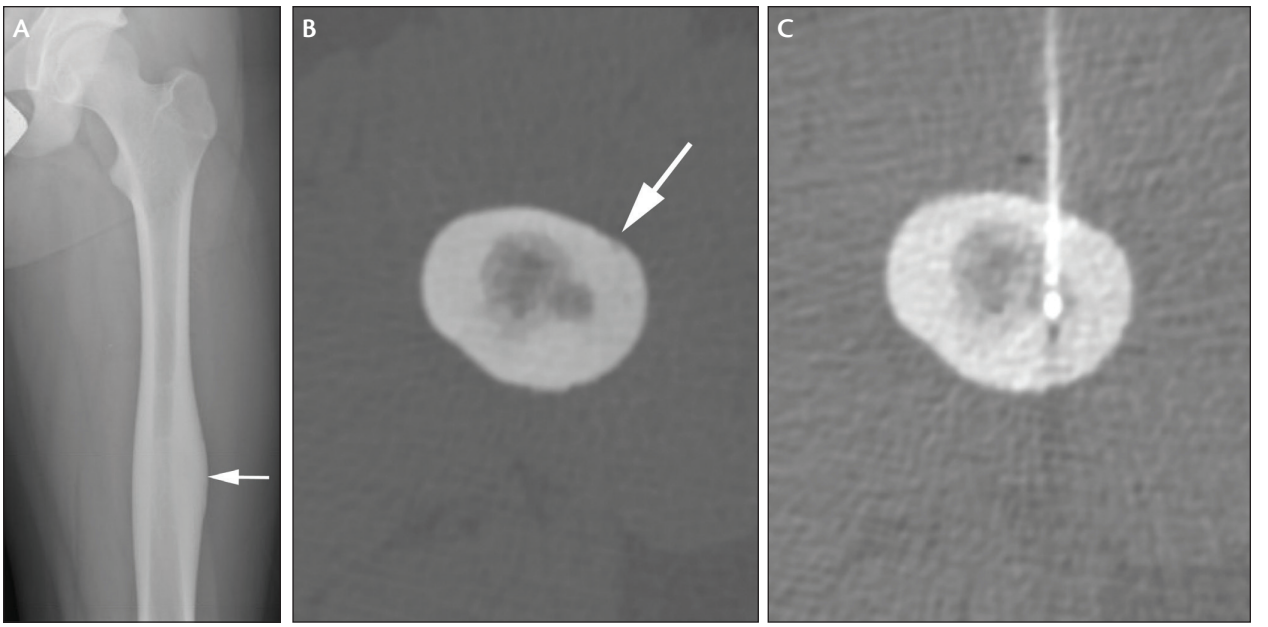

Figure 10. Left femur radiograph (A) and CT (B) demonstrating osteoid osteoma. Radiofrequency ablation probe placement (C) at the time of ablation.

marked on the skin using CT guidance (Figure 10B). The 14-gauge Bonopty penetration set (AprioMed, Inc.) was used to access the bone, a short drill was used to perforate the cortical bone, and a long drill was used to create a tract to the nidus. Then, a 16-gauge Bonopty biopsy needle was used to harvest tissue from the nidus, and the long drill was reinserted to create a tract extending beyond the nidus for the radiofrequency ablation probe. Finally, the 16-gauge radiofrequency ablation probe was inserted and placed in the center of the lesion (Figure 10C). Radiofrequency ablation was performed for 7 minutes, and a final temperature of 95° C was reached. At 1-year follow-up, the patient's thigh and knee pain had resolved. Radiofrequency ablation for osteoid osteoma is a safe, effective, and minimally invasive treatment approach, and recurrences of osteoid osteoma after treatment is uncommon.[11] ■

1. Park JS, Yoon DS, Kim KS, et al. What is the best treatment modality for adrenal metastasis from hepatocellular carcinoma? J Surg Oncol. 2007;96:32-36.
2. Lorenzin D, Pravisani R, Leo CA, et al. Complete remission of unresectable hepatocellular carcinoma after combined sorafenib and adjuvant yttrium-90 radioembolization. Cancer Biother Radiopharm. 2016;31:65-69.
3. Lee AJ, Gomes AS, Liu DM, et al. The road less traveled: importance of the lesser branches of the celiac axis in liver embolotherapy. Radiographics. 2012;32:1121-1132.
4. Burgmans MC, Kao YH, Irani FG, et al. Radioembolization with infusion of yttrium-90 microspheres into a right inferior phrenic artery with hepatic tumor supply is feasible and safe. J Vasc Interv Radiol. 2012;23:1294-1301.
5. Moustafa AS, Abdel Aal AK, et al. Chemoembolization of hepatocellular carcinoma with extrahepatic collateral blood supply: anatomic and technical considerations. Radiographics. 2017;37:963-977.
6. Paul SB, Gamanagatti SR, Mukund A, et al. Transarterial chemoembolization for hepatocellular carcinoma: significance of extrahepatic collateral supply. Indian J Cancer. 2011;48:339-344.
7. Cheng LF, Ma KF, Fan WC, et al. Hepatocellular carcinoma with extrahepatic collateral arterial supply. J Med Imaging Radiat Oncol. 2010;54:26-34.
8. Song SY, Chung JW, Kwon JW, et al. Collateral pathways in patients with celiac axis stenosis: angiographic-spiral CT correlation. Radiographics. 2002;22:881-893
9. Smolock A, Lubner MG, Ziemlewicz TJ, et al. Microwave ablation of hepatic tumors abutting the diaphragm is safe and effective. Am J Roengenol. 2015;204:197-203.
10. Hurwitz MD, Ghanouni P, Kanaev SV, et al. Magnetic resonance-guided focused ultrasound for patients with painful bone metastases: phase III trial results. J Natl Cancer Inst. 2014;106.
11. Virayavanich W, Singh R, O'Donnel RJ, et al. Osteoid osteoma of the femur in a 7-month-old infant treated with radiofrequency ablation. Skeletal Radiol. 2010;39:1145-1149.

Nicholas Fidelman, MD
Department of Radiology and Biomedical Imaging
University of California San Francisco
San Francisco, California
nicholas.fidelman@ucsf.edu
Disclosures: Research grant from Sirtex Medical, Inc.

Matthew D. Bucknor, MD
Department of Radiology and Biomedical Imaging
University of California San Francisco
San Francisco, California
Disclosures: None.

Paul Haste, MD
Department of Radiology and Biomedical Imaging
University of California San Francisco
San Francisco, California
Disclosures: None.

Maureen P. Kohi, MD
Department of Radiology and Biomedical Imaging
University of California San Francisco
San Francisco, California
Disclosures: None.

Ryan M. Kohlbrenner, MD
Department of Radiology and Biomedical Imaging
University of California San Francisco
San Francisco, California
Disclosures: None.

K. Pallav Kolli, MD
Department of Radiology and Biomedical Imaging
University of California San Francisco
San Francisco, California
Disclosures: None.

Kristen Lee, MD
Department of Radiology and Biomedical Imaging
University of California San Francisco
San Francisco, California
Disclosures: None.

Evan D. Lehrman, MD
Department of Radiology and Biomedical Imaging
University of California San Francisco
San Francisco, California
Disclosures: None.

Thomas M. Link, MD, PhD
Department of Radiology and Biomedical Imaging
University of California San Francisco
San Francisco, California
Disclosures: None.

Andrew G. Taylor, MD, PhD
Department of Radiology and Biomedical Imaging
University of California San Francisco
San Francisco, California
Disclosures: None.